IVYSPRING INTERNATIONAL PUBLISHER

Theranostics

2019; 9(12): 3580-3594. doi: 10.7150/thno.33141

Research Paper

An in situ microenvironmental nano-regulator to inhibit the proliferation and metastasis of 4T1 tumor

Huijuan Zhang[1,2,3], Xiaoge Zhang[1], Yanping Ren[1], Fang Cao[1], Lin Hou[1,2,3]✉, Zhenzhong Zhang[1,2,3]✉

1. School of Pharmaceutical Sciences, Zhengzhou University, Zhengzhou, China
2. Key Laboratory of Targeting Therapy and Diagnosis for Critical Diseases, Henan Province
3. Collaborative Innovation Center of New Drug Research and Safety Evaluation, Henan Province, Zhengzhou, China

✉ Corresponding author: Email address: zhangzz08@126.com (Zhenzhong Zhang), houlin_pharm@163.com (Hou Lin); Tel.: +86 371 6778 1910. Fax: +86 371 6778 1908. Mailing address: No.100, Kexue Road, Zhengzhou 450001, P. R. China

Received: 2019.01.14; Accepted: 2019.04.19; Published: 2019.05.26

Abstract

Tumor microenvironment, such as hypoxia and presence of immune cells, plays a critical role in cancer initiation, growth as well as progression, and seriously affects antitumor effect. Accordingly, we constructed a kind of multifunctional nanoparticles (NPs) with macrophage transformation and oxygen (O_2) generation characteristics, to regulate the tumor microenvironment.

Methods: In this study, we synthesized mesoporous Prussian blue (MPB) NPs with low molecular weight hyaluronic acid (LMWHA) surface modification (LMWHA-MPB), and discovered that LMWHA-MPB could be used as an in situ macrophages converter and O_2 generator.

Results: *In vitro* results showed after uptake by M2 macrophages, LMWHA-MPB displayed the potential in remodeling tumor-associated macrophages (TAMs) phenotype (pro-tumor M2→anti-tumor M1), and anti-metastatic effect on 4T1 cells. Furthermore, *in vivo* visualized near-infrared (NIR) imaging data proved IR783 labeled LMWHA-MPB NPs could selectively accumulate in tumor sites. Then plenty of O_2 generated to alleviate tumor hypoxia via catalytic decomposition of endogenous hydrogen peroxide (H_2O_2). Based on these outstanding characteristics, LMWHA-MPB NPs were adopted as multifunctional nanocarriers to load sonosensitizer hematoporphyrin monomethyl ether (HMME) for O_2 self-provided sonodynamic therapy (SDT). *In vivo* anti-tumor results showed LMWHA-MPB/HMME could effectively inhibit the proliferation and metastasis of 4T1 tumors by improving tumor microenvironment.

Conclusion: The multifunctional NPs can be used as in situ microenvironmental nano-regulators to inhibit the proliferation and metastasis of 4T1 tumor.

Key words: mesoporous Prussian blue, low molecular weight hyaluronic acid, tumor microenvironment, SDT, tumor associated macrophages

Introduction

In the past few years, studies have revealed that as an integral part of tumor physiology, tumor microenvironment plays a critical role in cancer initiation, growth, and progression [1-3]. The intrinsic features of tumor microenvironment, such as pH, glutathione (GSH), growth factors, oxygen levels and presence of immune cells, have been increasingly considered as specific targets for drug delivery, cancer diagnosis therapeutics and prognosis [4-7].

Tissue oxygenation is an important component of microenvironment and can acutely alter the behaviors of cells, such as cell survival, apoptosis, glucose metabolism, and angiogenesis [8]. In normal tissues, O_2 levels span from 150 mm Hg to 20-70 mm Hg, whereas markedly lower levels (≤ 2.5 mm Hg) have been described in most types of locally advanced tumors [1]. This is because the abnormal vessels within tumor tissues and rapid proliferation of tumor

cells can cause an imbalance between O_2 supply and consumption. Various investigations have clearly demonstrated that hypoxia causes a challenge for cancer therapy [9-10]. It not only contributes to tumor proliferation, metastasis and angiogenesis, but also induces resistance to many types of tumor therapeutics [11], particularly for O_2 based photodynamic therapy (PDT) or SDT [12]. Up to now, several strategies have been proposed to overcome tumor hypoxia and then enhance tumor treatment efficiency, such as increasing O_2 supply using perfluorocarbon-loaded nanoparticles [13-14], promoting tumor oxygenation through chemical or biochemical reactions locally [15-17], enlarging intratumor blood flow [18], or hypoxia-medicated prodrugs activation [19-20]. However, these methods cannot be applied to clinic because of their potential safety concerns, limited O_2-carrying capacities and poorly O_2-delivering efficiency in hypoxic tumor region. How to take advantage of the tumor's own characteristics to generate O_2 continuously in situ, maybe a new and effective strategy to solve hypoxia fundamentally.

High accumulation of macrophage (tumor associated macrophages, TAMs) in hypoxic regions of solid tumor is another important component of microenvironment [1]. Normally, macrophages present two subtypes, classically activated pro-inflammatory macrophages (M1) and alternatively activated anti-inflammatory macrophages (M2). The polarization of these two macrophages is a highly dynamic process [2]. They can be reversed with stimulation of different environmental or biological factors. Initially, TAMs present a M1-like phenotype in tumor inflammation areas, which exhibit anti-tumor activity by secreting pro-inflammatory cytokines (such as tumor necrosis factor (TNF), IL-6, IL-12, IL-23), reactive nitrogen and oxygen species (such as H_2O_2, NO, superoxide) [21]. Thereafter, M1 macrophages are transformed into M2-like phenotype responding to secreted cytokines, chemokines, growth factors and stress signals in the tumor microenvironment. M2 macrophages secrete pro-tumor cytokines (such as IL-4, IL-10, IL-13) and alter gene expression (such as up-regulation hypoxia-inducible factor (HIF), vascular endothelial growth factor (VEGF) and matrix metalloproteinase 7 (MMP-7)), to promote tumor progression [21]. Studies demonstrate that there is a high density of M2 macrophages in tumor hypoxia region [1]. Therefore, synchronous remodeling macrophage phenotype (M2 to M1) and alleviating tumor hypoxic microenvironment may be a new and efficient strategy for tumor treatment [22].

Cancer cells have been found to generate oxidative stress by inducing an elevated level of H_2O_2 [23-24]. The utilization of H_2O_2-catalysts to decompose endogenous H_2O_2 into O_2 has been recognized to be an attractive strategy to relieve tumor hypoxia and improve cancer therapeutic efficacy [12]. Prussian blue (PB) has been approved by USA Food and Drug Administration (FDA) as a safe and clinical medicine for the treatment of radioactive exposure. Previous studies have proved that PB NPs also have excellent catalase activity [25]. Therefore, ensuring adequate supplement of endogenous H_2O_2 substrate is the key to lessen tumor hypoxia. Hyaluronic acid (HA) polysaccharose with different molecular weights can promote differential inflammatory mediators and signals [26]. Rayahin et al. proved that HA has molecular weight-dependent effects on modulating macrophage phenotype. Macrophages exposed to LMWHA are encouraged to produce pro-inflammatory mediators associated with the classically activated state [27]. In this study, we modified MPB NPs with LMWHA to remodel TAMs phenotype (pro-tumor M2 → anti-tumor M1), guaranteeing continuous supplement of H_2O_2 substrate in the tumor hypoxic area. Combing with the specific catalysis of MPB NPs, there is steady O_2 generation within tumor to alleviate hypoxia. After loading sonosensitizer HMME, LMWHA-MPB/HMME can effectively inhibit the proliferation and metastasis of 4T1 tumor (**Figure 1)**.

Experiment Section

Materials

Low molecular weight sodium hyaluronate (LMWHA, purity > 98%, MW = 6276) was obtained from Bloomage Freda Biopharm Co. Ltd (Jinan, Shandong, China). Fluorescein isothiocyanate (FITC), 1-Ethyl-3-(3-dimethyllaminopropyl) carbodiimide hydrochloride (EDC·HCl), N-Hydroxysuccinimide (NHS) and Sulforhodamine B (SRB) were got from Sigma-Aldrich (St Louis, MO, USA). Hematoporphyrin monomethyl ether (HMME, purity > 98%) was sourced from Shanghai biological technology Co., Ltd (Shanghai, China). Polyethyleneimine (PEI, purity > 99%, MW = 10000) was purchased from Xiya Reagent Research Center (Jinan, Shandong, China). Potassium ferrocyanide ($K_3Fe(CN)_6$, purity > 99.5%) was obtained from Shandong haozhong chemical technology Co., Ltd (Shandong, China) and polyvinyl pyrrolidone (PVP K30, purity > 98%) was bought from Tianjin regent chemicals Co., Ltd (Tianjin, China). Recombinant murine IL-4, rabbit Anti-CD86/PE (bs-1035R-PE) and Anti-CD206/FITC (bs-2664R-FITC) were purchased from Beijing Biosynthesis Biotechnology Co. Ltd

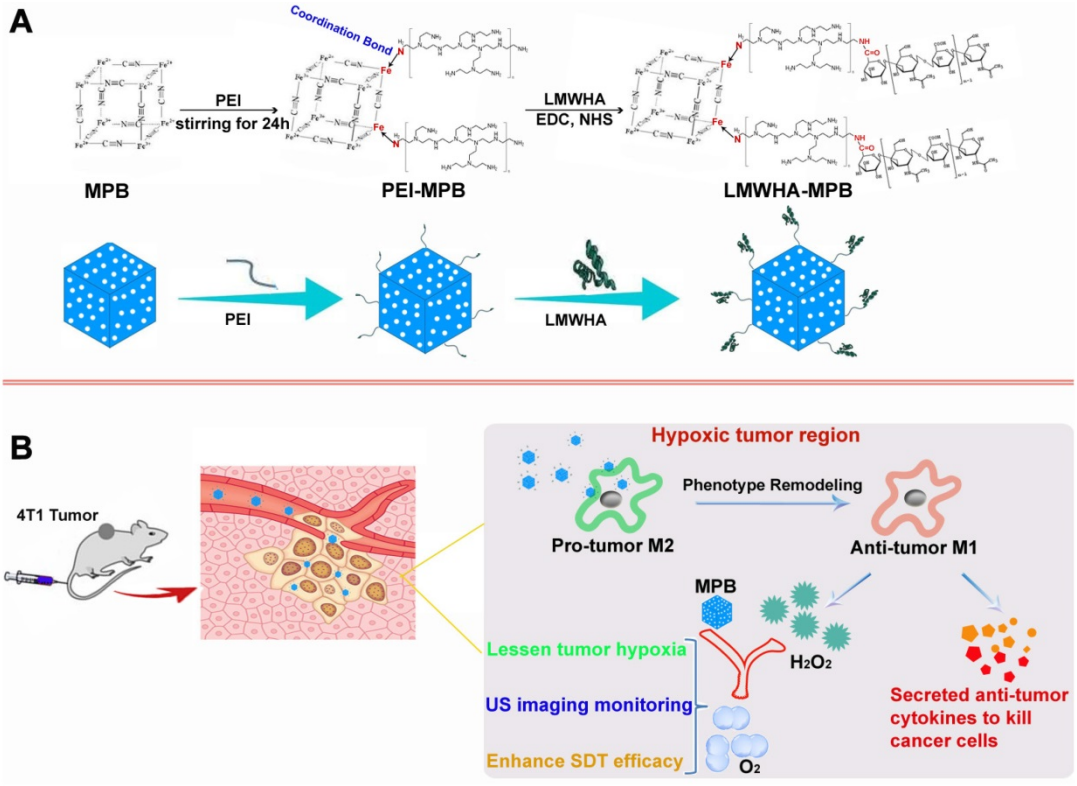

Figure 1. (**A**) The synthetic scheme of LMWHA-MPB nanoparticles. (**B**) Schematic illustration of HMME-loading LMWHA-MPB nanoparticles to inhibit the proliferation and metastasis of 4T1 tumor *in vivo*.

(Beijing, China). MMP-9 and VEGF ELISA Kits were bought from Dakewe Biotech Co., Ltd. (Beijing, China). IL-10 and IL-12 ELISA kits were bought from Thermo Fisher Scientific (Shanghai, China).

Synthesis of LMWHA-MPB

The synthesis of MPB NPs was conducted according to a previous reported procedure [28]. Firstly, PVP K30 (3.0 g) and $K_3[Fe(CN)_6]$ (132 mg) were added to 40 mL of 0.01 M HCl solution under magnetic stirring at room temperature, to form transparent solution. The vial was placed into an electric resistance furnace and heated at 80 °C for 24 h. Then the mixture was centrifuged at 12000 r/min for 30 min at 4 °C to collect PB NPs. After purification with deionized water, solid PB NPs were obtained after drying at 80 °C. Next, 20 mg of above-mentioned PB NPs were added into 20 mL of 1.0 M HCl solution containing 100 mg of PVP K30. After magnetic stirring for 5 h at room temperature, the vial was placed into an electric resistance furnace and heated at 140 °C for 4 h. Then the mixture was centrifuged at 12000 r/min for 30 min at 4 °C to collect MPB NPs. After purification with deionized water, MPB NPs were freeze-dried in vacuum for 24 h.

50 mg of MPB NPs were dispersed into 50 mL of water. Then 30 mg of PEI was added and magnetically stirred for 24 h. The mixture was dialyzed for 24 h to remove free PEI, and then the products (PEI-MPB NPs) were freeze-dried in vacuum for 48 h. Next, PEI-MPB NPs (50 mg) and LMWHA (50 mg) were dispersed into 50 mL of formamide solution containing 346 mg of EDC·HCl and 206 mg of NHS under magnetic stirring. Then 180 μL of triethylamine was added to this activated mixture drop by drop in the ice bath, followed by stirring for 12 h at room temperature. The pre-cooled acetone was added into the reaction solution to precipitate LMWHA-MPB NPs. After centrifugation, the precipitation was re-dissolved with water and dialyzed with a dialysis bag (MW = 12000) for 24 h to remove EDC·HCl, NHS and free LMWHA. The synthetic products (LMWHA-MPB) were freeze-dried in vacuum for 48 h.

HMME loading on LMWHA-MPB and drug content determination

0.5 mg/mL of LMWHA-MPB dispersions were prepared using ultrasonic techniques. Different concentrations of HMME (0.25, 0.5, 1, 1.5 mg/mL) were added into the above dispersion. After stirring for 24 h, the suspension was dialyzed for 12 h (MW = 3500) in dialysate (ethanol:water = 1:9) to remove unloaded HMME. To measure loading efficacy, dilute LMWHA-MPB/HMME nanosuspension with 30 times the volume of methanol and sonicate to ensure loading drug dissociation completely. Then centrifuge

to separate LMWHA-MPB and HMME. Calculate the concentration of loaded HMME in the supernatant by high performance liquid chromatography (HPLC) method. HPLC was performed on a Symmetry ® C18 column with mobile phase: methanol/acetonitrile/ PBS buffer solution (pH = 6.9): 30/20/50; fluorescence detector set: λex = 395nm and λem = 613nm. The entrapment efficiency (EE) and loading efficiency (LE) were calculated using formula 1 and 2, respectively.

$$\text{Entrapment efficiency (\%)} = \text{WLoaded HMME} / \text{WTotal HMME} \times 100\% \quad (1)$$

$$\text{Loading efficiency (\%)} = W_{\text{Loaded HMME}} / (W_{\text{Loaded HMME}} + W_{\text{LMWHA-MPB}}) \times 100\% \quad (2)$$

Characterization

Morphological feature of nanoparticles was monitored by the transmission electron microscopy (TEM). The spectral features were monitored with an ultra-violet visible absorption spectrometer (UV-vis) and the Fourier transform infrared spectrometer (FTIR). The particle size and zeta potential were determined by a laser diffraction-based particle size analyzer (DLS).

Treat RAW264.7 cells with IL-4 to generate M2 macrophages

With reference to classic methods, RAW264.7 cells were seeded in 6-well plates with a density of 1.0×10^5 cells per well and incubated for 24 h. Subsequently, 40 ng/mL of IL-4 was added into the wells and incubated with RAW264.7 cells for 24 h, to induce RAW264.7 cells converting to M2-type macrophages. Then a typical marker for M2 phenotype, CD206/FITC dye was used to stain M2 macrophages. Flow cytometric analysis was performed to quantify the conversion ratio.

Internalization of LMWHA-MPB by M2 macrophages

To investigate whether LMWHA modified MPB NPs could enhance the targeting ability to M2-type macrophages, RAW264.7 cells pretreated with IL-4 were incubated with FITC-labeled MPB and LMWHA-MPB (FITC: 2 μg/mL; MPB: 10 μg/mL; LMWHA-MPB: 10 μg/mL) for 0.5, 1 and 2 h, respectively. After being washed with PBS, cells were fixed with 4% paraformaldehyde and stained with DAPI (2.0 μg/mL) for 15 min. Laser confocal microscope was used to record the results. Moreover, in order to quantitative determination of internalized nanoparticles, after treated with FITC-labeled MPB and LMWHA-MPB for 0.5, 1 and 2 h, cells were washed and collected for flow cytometry detection.

Modulation of M2-type macrophages towards M1-type phenotype with LMWHA-MPB *in vitro*

RAW264.7 cells were seeded in 6-well plates with a density of 1.0×10^5 cells per well and incubated for 24 h, followed by incubation with fresh culture medium containing 40 ng/mL of IL-4 for 24 h. Then treat cells with LMWHA-MPB (50 μg/mL) for 1 h and 3 h, respectively. After that, culture medium containing formulations was removed and 200 μL of fresh culture medium containing CD86/PE dye was added. After incubation for 2 h, cells were washed twice with PBS. After trypsinization and centrifugation, cells were collected and suspended in PBS buffer for flow cytometry analysis.

Determination of IL-10 and IL-12 concentrations in macrophages

RAW264.7 cells were treated with 40 ng/mL of IL-4 for 24 h to induce the polarization of M0 to M2 phenotype. Then M2 macrophages were incubated with LMWHA-MPB (50 μg/mL) for 3 h to induce the polarization of M2 to M1 phenotype. After incubation with serum-free medium for 24 h, the cell culture mediums of each group were collected. The concentrations of IL-10 and IL-12 in the supernatant secreted by these three kinds of macrophages were determined with mouse IL-10 and IL-12 ELISA kits, respectively.

Transwell Motility and Invasion Assay *in vitro*

M2 macrophages induced by IL-4 were incubated for 24 h, and then old medium were replaced with fresh medium containing 50 μg/mL of MPB or LMWHA-MPB. After incubation for 4 h, the medium was collected as conditioned medium. Meanwhile, M2 medium without administration was also collected and used as M2 conditioned medium.

Wound-healing migration assay was used to detect the migration ability of 4T1 tumor cells after LMWHA-MPB NPs and M2 macrophages were co-cultured. Briefly, 4T1 cells were seeded into 6-well plates at a density of 1×10^5 cells per well. After incubation for 24 h, cell monolayers were carefully wounded with a 200 μL pipette tip, washed with serum-free medium and exposed to the above-mentioned conditioned medium for different times. Cell treated with fresh and serum-free medium was used as the control group. The photographs of the wound areas were recorded using a fluorescence microscope (Zeiss LSM 510) after incubation for 0 and 18 h. Migration rate of 4T1 cells was calculated by the formula Migration rate = [(Scratch width at 0 h - Scratch width at 18 h)/ Scratch width at 0 h] × 100%.

Transwell experiment was used to evaluate the effect on tumor cell invasion and metastasis ability

after LMWHA-MPB NPs and M2 macrophages were co-cultured. 4T1 cells were seeded into the upper compartment transwell (8.0 μm pore size) pre-coated with matrigel at a density of 5×10^4 cells per well and treated with serum-free medium, M2 conditioned medium, MPB pre-treated M2 conditioned medium and LMWHA-MPB pre-treated M2 conditioned medium, respectively at 37 °C. The lower chamber was filled with 800 μL of medium containing 10% FBS. After incubation for 24 h, un-migrated cells on the upper side of the membrane were washed and removed. The migration cells in the lower surface of the membrane were fixed, stained with 0.1% crystal violet solution and photographed in different view fields under a microscope (Zeiss LSM 510). Next, the crystal violet staining cells were dissolved in 35% acetic acid and their absorbance was measured at 560 nm to determine the invasion and metastasis ability of 4T1 cells. Invasion ability = OD value of experimental group / OD value of control group.

The sonodynamic therapy effect of HMME loaded LMWHA-MPB *in vitro*

Preparation of conditioned medium. M2 macrophages induced by IL-4 were incubated for 24 h, and then old medium were replaced with fresh medium containing MPB, LMWHA-MPB, HMME, MPB/HMME and LMWHA-MPB/HMME (MPB and LMWHA-MPB: 50 μg/mL; HMME: 30 μg/mL), respectively. After incubation for 4 h, the medium was collected as conditioned medium.

SRB assay was performed to evaluate the cytotoxicity of nanoparticles. 4T1 cells were seeded at a density of 5.0×10^3 cells per well in 96-well plates and cultured for 24 h. Then old medium was replaced with the above-described conditioned medium. At 4 h after administration, cells in control (normal medium), HMME, MPB/HMME and LMWHA-MPB/HMME groups were exposed to ultrasound (3 MHZ, 1.0 W/cm^2, 0.5 min). Subsequently, cells were incubated for 24 h, and then standard SRB assay was conducted to evaluated cell viabilities.

Furthermore, in order to visualize the sonodynamic cytotoxicities, calcein-AM/PI double staining experiment was also conducted for assessment of cellular viability. Grouping and processing methods were as above. After ultrasound irradiation, cells were incubated for 24 h. Cells were washed with PBS for several times, followed by incubating with calcein AM (0.67 μM) and PI (1.5 μM) for 15 min at 37 °C with 5% CO_2. Finally, the cells were washed twice with PBS and then fluorescence images were acquired under a fluorescence microscope (Zeiss LSM 510).

The sonodynamic therapy effect of HMME loaded LMWHA-MPB *in vivo* on 4T1 tumor-bearing model

All animal experiments were performed under protocols approved by Henan laboratory animal center. 2×10^6 4T1 cancer cells were injected subcutaneously into the right upper limb of the female mice (BALB/c), to build the subcutaneous 4T1 breast cancer xenografts. When the tumor volume reached average size of 100 mm^3, mice were used for *in vivo* experiments.

In vivo visualized NIR imaging

4T1 tumor-bearing mice were randomly allocated into three groups: (a) IR783 and (b) LMWHA-MPB/IR783 (IR783: 1.0 mg/kg). Various formulations were intravenously injected into the tail vein of the mice. At different time points, fluorescent images were acquired using an *in vivo* imaging system FX PRO (Kodak, USA). The excitation wavelength and emission wavelength were 700 nm and 830 nm, respectively. After 24 h post injection, tumors and major organs of each group were excised to record their fluorescence intensity.

Ultrasound imaging based on oxygen production

For *in vivo* imaging, 4T1 tumor-bearing mice were randomly divided into three groups (n = 5): (1) N.S., (2) MPB, (3) LMWHA-MPB. The dose administered to mice was 10 mg/kg. At predetermined time points after intravenous administration, the Vevo2100 small animal US imaging system was used to obtain US images of the tumor sites. For *in vitro* imaging, add MPB NPs dispersion into H_2O_2 solution with the final concentration of MPB and H_2O_2 being 10 μg/mL and 2 mM, respectively. These samples were placed in EP tubes. The signals were recorded using a small animal ultrasound imager.

Anti-tumor effect *in vivo*

4T1 tumor-bearing mice were randomly divided into seven groups (n = 5): (1) N.S., (2) MPB, (3) LMWHA-MPB, (4) N.S.+US, (5) HMME+US, (6) MPB/HMME+US, (7) LMWHA-MPB/HMME+US. All formulations were intravenously administrated every 2 days for 6 times with the same HMME dose (10 mg/kg) and nanocarriers (MPB or LMWHA-MPB) dose (10 mg/kg). For (4) to (7) groups, the tumor sites of mice were exposed to ultrasound (3 MHz, 1.0 W/cm^2) for 1.0 min after 2 h post-injection. The tumor size was measured every two days with vernier calipers and tumor volume was calculated by the formula $V = [(\text{length}) \times (\text{width})^2]/2$. In addition, the

toxicity of the above formulations was monitored by investigating animal behavior and body weight. The treatment period lasted for 12 days. At the end of the pharmacodynamics experiment on the 12th day, tumor tissues of each group were excised and soaked in 10% formalin solution, embedded with paraffin for hematoxylin and eosin (H&E) staining and immunohistochemical staining (Ki67 and MMP-9). Furthermore, the lung tissues in N.S, LMWHA-MPB and LMWHA-MPB/HMME+US groups were isolated and soaked in Bouin's solution for 24 h and dehydrated in absolute ethyl alcohol for the quantification of visible metastatic pulmonary nodules, to evaluate the pulmonary metastasis of 4T1 tumor.

Immunofluorescence

At the end of pharmacodynamic experiment, tumor tissues of each group were subjected and soaked in 10% formalin solution, embedded with paraffin for immunofluorescence staining. To evaluate tumor hypoxia, Hypoxyprobe™-1 Plus Kits (FITC-Mab) hypoxia probe was used to detect the hypoxia area of the tumor tissues in each group. To determine the effect of LMWHA-MPB nanoparticles on the polarization of TAMs, rabbit polyclonal FITC-CD206 antibody (dilution 1:50) and rabbit polyclonal PE-CD86 antibody (dilution 1:50) were used to determine the distribution of M2 and M1 macrophages in tumor tissues, respectively.

In vivo toxicity evaluation

The toxicity of the formulations is evaluated on health mice. Briefly, the health mice were randomly divided into 6 groups (n = 3): (1) N.S., (2) MPB, (3) LMWHA-MPB, (4) HMME, (5) MPB/HMME, (6) LMWHA-MPB/HMME. All formulations were intravenously administrated every 2 days for 6 times with the same HMME dose (10 mg/kg) and nanocarriers (MPB or LMWHA-MPB) dose (10 mg/kg). At the 12th day, the toxicity of the formulations was evaluated by the serum biochemistry assay and histological examination.

Statistical Analysis

All experimental data were shown as mean ± SD, and differences between two groups were analyzed by SPSS software via one-way ANOVA.

Results and Discussion

Synthesis and characterization of LMWHA-MPB

Firstly, PVP K30 was used as template to synthesize PB NPs. TEM image clearly exhibited the cubic structure and smooth surface of PB NPs (**Figure 2A**). The typical -C≡N stretching vibration peak at 2087.15 cm^{-1} and -Fe-C≡N-Fe bending vibration peak at 500.93 cm^{-1} in FTIR spectrum (**Figure S1**), belonging to the structural composition of PB [28], were further confirmed the successful preparation of PB NPs. Then MPB NPs were prepared via a controlled acid self-etching reaction. TEM image demonstrated that MPB showed excellently internal porous structure (**Figure 2B**), allowing small drug molecules (such as HMME) to freely diffuse into the porous interior of MPB. Dynamic light scattering analysis showed the average diameter of MPB NPs was ~91 nm with uniform particle size distribution (**Figure 2C and Figure S2**). The zeta potential of MPB NPs was -10.1 mV (**Figure S3**). **Figure S4** showed the size and PDI changes of MPB NPs in PBS and cell medium, suggesting that MPB NPs could be stable for one week in physiological solutions.

It's reported that HA is an immuno stimulant and has immunotoxicological effect on macrophages. Particularly, LMWHA can activate the polarization of M2-type macrophages to M1-type macrophages. Herein, LMWHA was utilized to modify the surface of MPB NPs, which can also improve the biocompatibility and stability of MPB. The synthesis procedure of LMWHA-MPB was illustrated in **Figure 1,** and **Figure 2D** showed the FTIR spectrum of LMWHA-MPB. The typical C=O stretching vibration band at 1728.97 cm^{-1}, N-H bending modes at 1645.77 cm^{-1} and C-N stretching vibration band at 1384.03 cm^{-1}, all suggested that the amide bond between LMWHA and MPB (with PEI-amino groups) was synthesized successfully. After LMWHA grafting, the particle size and zeta potential of LMWHA-MPB NPs were changed to ~127 nm (**Figure 2E and Figure 2F**) and -19.2 mV (**Figure 2G**). Figure S5 demonstrated the monodispersity of LMWHA-MPB NPs in aqueous phase. The size stability of LMWHA-MPB NPs in PBS and cell medium had been tested. The size and PDI changes shown in Figure S6 suggested that LMWHA-MPB NPs could be stable for one week in physiological solutions. The mesoporous structure made MPB an ideal carrier to encapsulate anticancer drugs, such as HMME. **Figure S7** showed the characteristics of HMME-loaded LMWHA-MPB. The drug loading efficiency improved from 22.9% to 63.4% along with increased HMME feeding amount, while entrapment efficiency exhibited firstly increased and then decreased trend. Finally, a feed ratio of 1:2 (LMWHA-MPB:HMME) was chosen for further studies with excellent drug loading efficiency (57.6%) and high entrapment efficiency (67.9%). The final zeta potential of LMWHA-MPB/HMME was -35.2 mV.

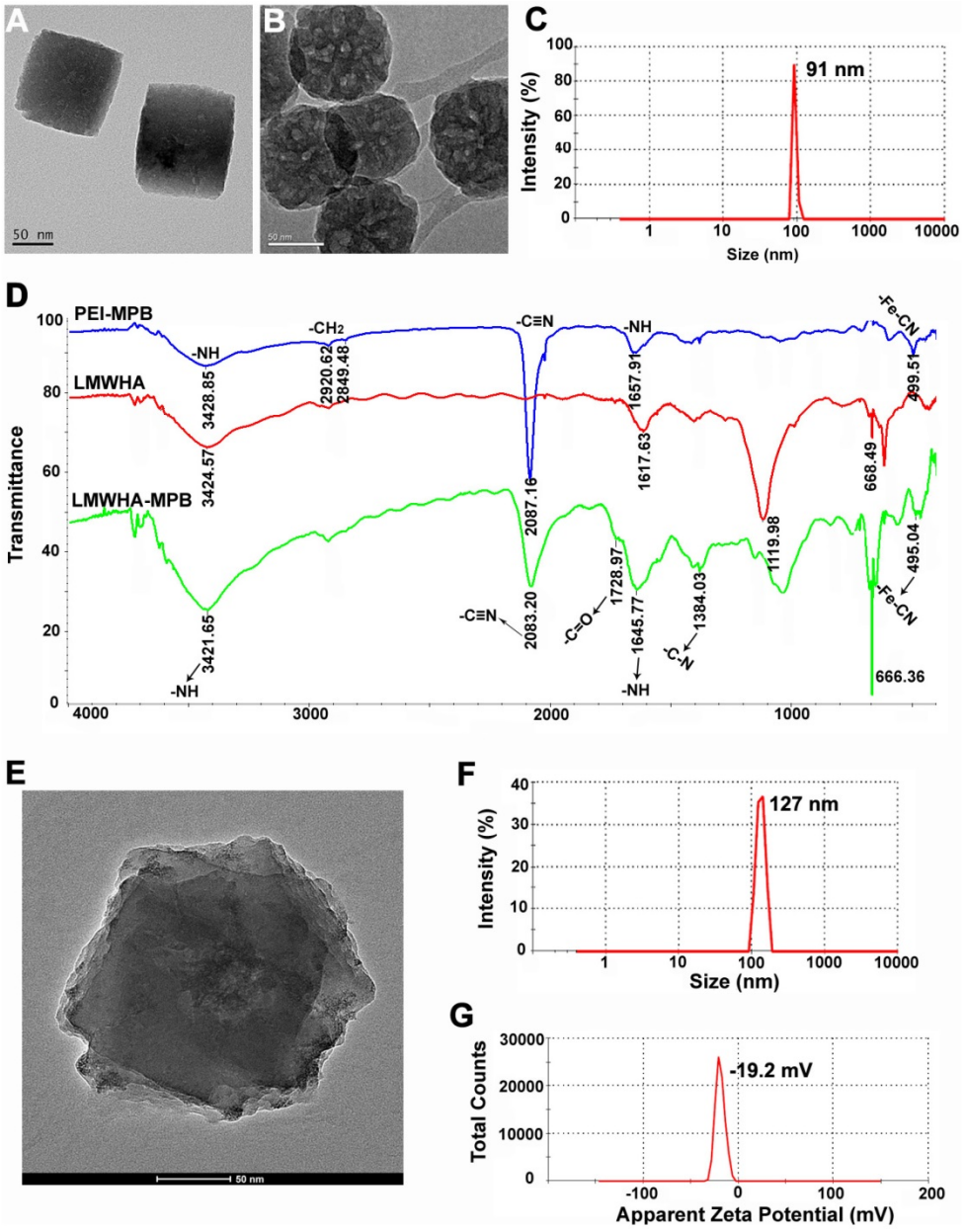

Figure 2. (**A**) TEM image of PB NPs. (**B**) TEM image of MPB NPs. (**C**) Particle size distribution of MPB NPs. (**D**) FTIR spectrum of PEI-MPB, LMWHA and LMWHA-MPB. (**E**) TEM image of LMWHA-MPB NPs. (**F**) Particle size distribution of LMWHA-MPB NPs. (**G**) Apparent zeta potential of LMWHA-MPB.

The remodeling regulation effect of LMWHA-MPB on macrophage phenotype

In order to explore the macrophages remodeling effect of LMWHA-MPB *in vitro*, firstly we induced RAW264.7 cells into M2 phenotype using IL-4. After incubation with IL-4 for 24 h at 40 ng/mL, FITC labeled CD206, a typical marker for M2 phenotype, was used to identify M2 macrophages (**Figure 3A**). Flow cytometry quantitative analysis showed ~83.1% macrophages were successfully induced to M2 phenotype. Subsequently, we found LMWHA modified MPB NPs were more easily internalized by M2 macrophages (**Figure 3B**). After incubation M2 macrophages with FITC-labeled MPB and LMWHA-MPB for 2 h, the fluorescent intensities within cells were 64.8% and 100.0%, respectively (**Figure S8**). This significant difference suggested a specific and rapid internalization of LMWHA-MPB by M2 macrophages. This may be due to the highly expressed HA receptors on the membrane of M2 macrophages [29]. It is known that HA has immunotoxicological effect, which can activate macrophages. Richard et al. have proved that LMWHA can induce a classically activated-like state (M1) or remodel TAMs phenotype from M2 to M1 by up-regulation of pro-inflammatory genes, including NOS 2, TNF, IL12b, and CD80, and enhancing

secretion of nitric oxide (NO) and TNF-α [27]. So, would LMWHA-MPB NPs have immunological effect on macrophage polarization after entering M2 macrophages? Next, we made further exploration. After treating M2 phenotype with LMWHA-MPB NPs for different hours, PE labeled CD86 was used to identify M1 macrophages. As **Figure 3C** shown, CD86 expression was significantly increased after incubation with LMWHA-MPB for 3 h, indicating that LMWHA-MPB could change the polarization from M2 to M1 phenotype. Moreover, the remodeling regulation effect of LMWHA-MPB on macrophage phenotype was further confirmed according to determining those correlated cytokines. As seen in **Figure 3D** and **3E**, after incubation with LMWHA-MPB for 3 h, the concentration of IL-10, a typical cytokine secreted by M2 macrophages, decreased obviously. While the secretion level of IL-12, the typical cytokine of M1 macrophages, increased significantly. All above results suggested the successful polarization of M2 to M1 phenotype by LMWHA-MPB NPs.

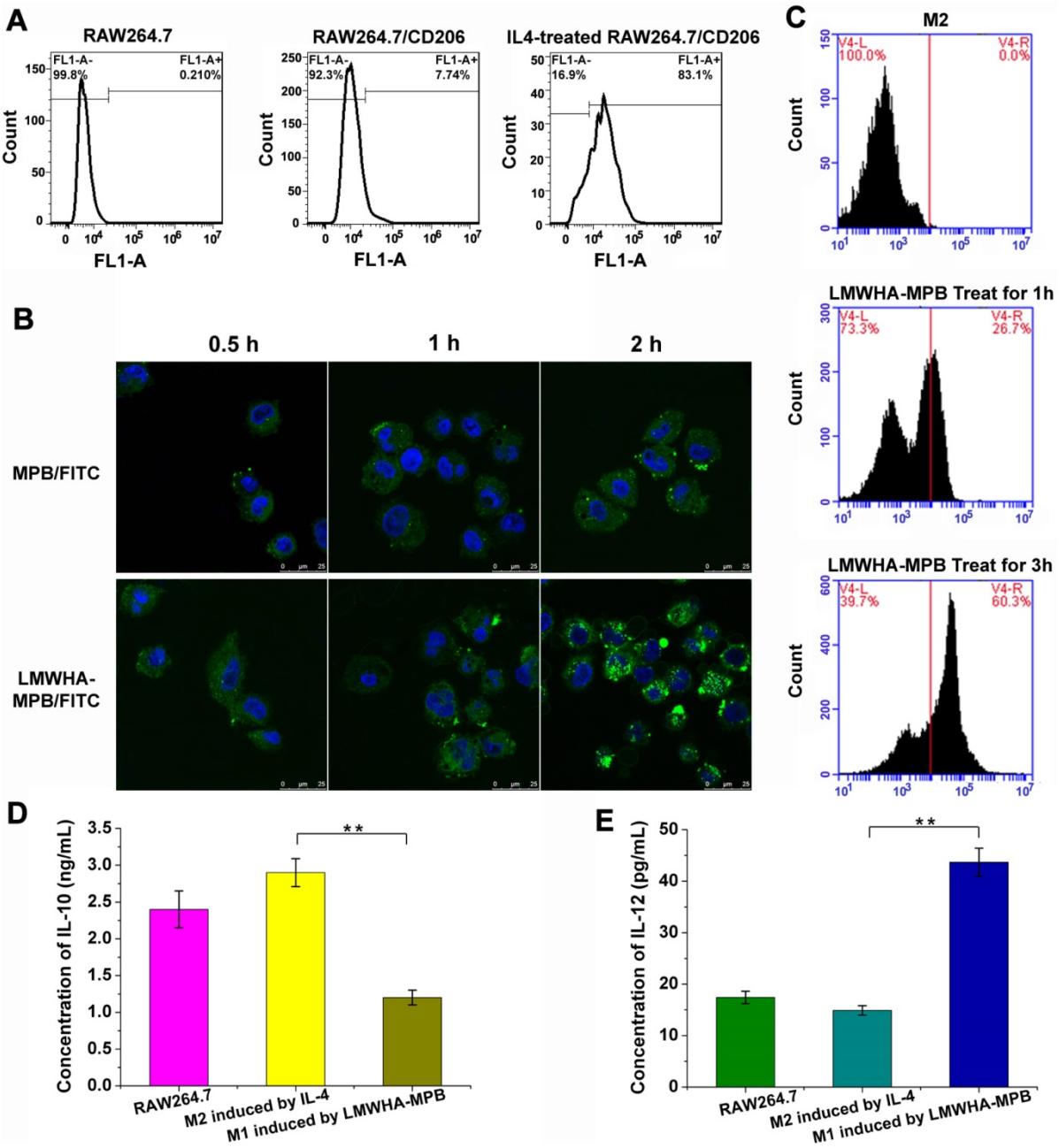

Figure 3. (**A**) The conversion ratio of RAW264.7 toward to M2 phenotype induced by interleukin-4 (IL-4). (**B**) The cellular uptake images of FITC-labeled nanoparticles by M2 macrophages. (**C**) Modulation of M2-type macrophages towards M1-type phenotype with LMWHA-MPB *in vitro* for 1 h and 3 h. M1 macrophages were labeled with CD86/PE dye. (**D**) The level of IL-10 secreted by macrophages before and after modulation of M2-type macrophages towards M1-type phenotype with LMWHA-MPB for 3 h. (**E**) The level of IL-12 secreted by macrophages before and after modulation of M2-type macrophages towards M1-type phenotype with LMWHA-MPB for 3 h. (*P < 0.05 and **P < 0.01).

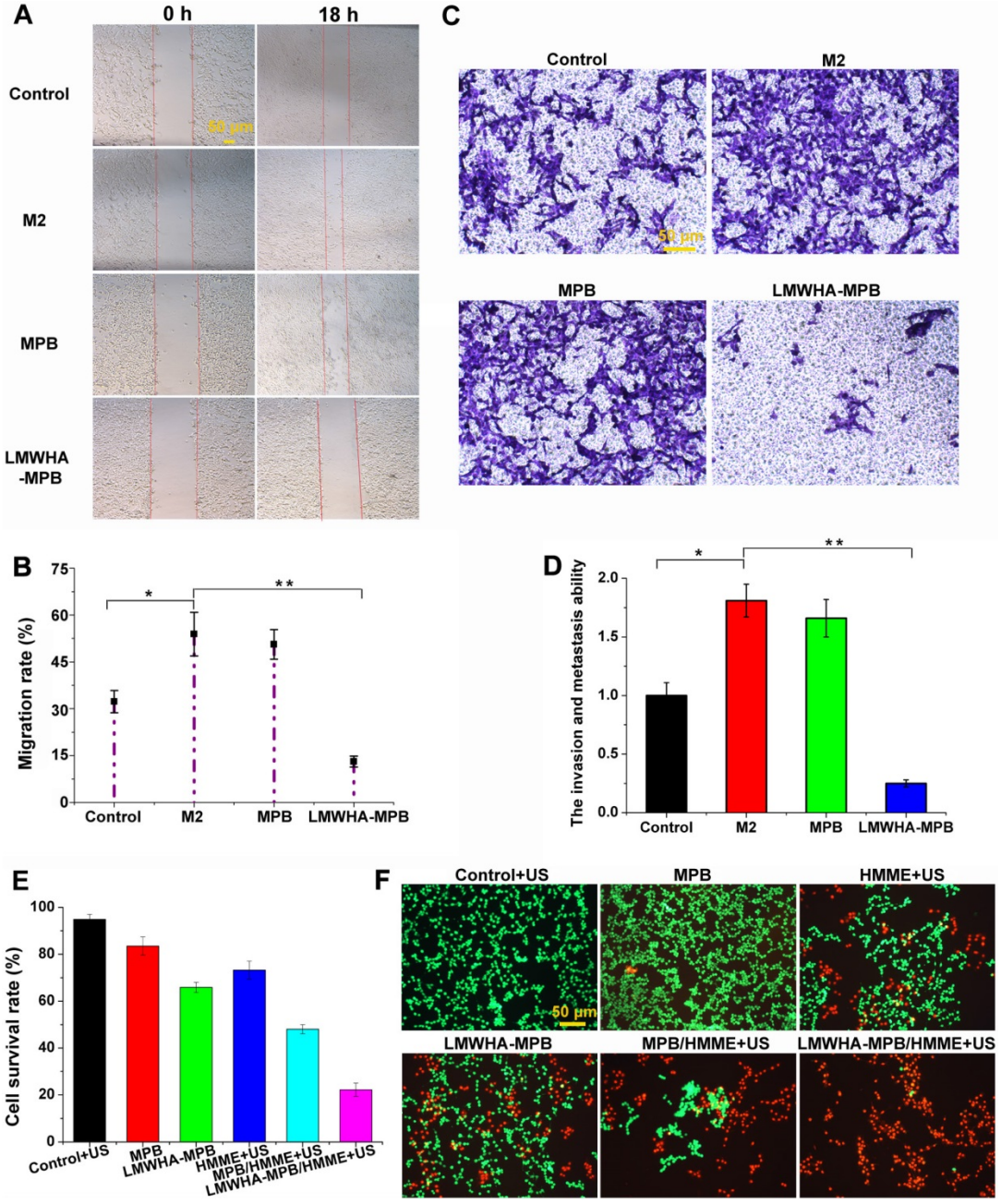

Figure 4. (**A**) Wound healing images after scratch for 0 h and 24 h. 4T1 cells incubation with fresh and serum-free medium were used as control group. In other groups, 4T1 cells were treated with M2 conditioned medium, MPB pre-treated M2 conditioned medium and LMWHA-MPB pre-treated M2 conditioned medium, respectively. (**B**) Migration rates of 4T1 cells incubation with different conditioned medium, evaluating by measuring the migration width. (**C**) Transwell assay images of 4T1 cells after treated with M2 conditioned medium, MPB pre-treated M2 conditioned medium and LMWHA-MPB pre-treated M2 conditioned medium, respectively. 4T1 cells incubation with fresh and serum-free medium were used as control group. (**D**) The invasion and metastasis ability of 4T1 cells incubation with different conditioned medium. (**E**) The *in vitro* sonodynamic therapy effect of MPB, LMWHA-MPB, MPB/HMME+US, LMWHA-MPB/HMME+US and HMME+US on 4T1 cells. (**F**) Calcein AM and PI staining results (green: live cells; red: dead cells). (*P < 0.05 and **P < 0.01).

In vitro cell migration and invasion assay

As we known, M1 and M2 polarized macrophages differ in many aspects of tumor progression. M2 macrophages are tumor-promoting phenotype which account for tumor proliferation and metastasis, while M1 macrophages are tumor-killing phenotype that inhibit tumor proliferation by secreting pro-inflammatory cytokines (such as TNF, IL-6, IL-12, IL-23), reactive nitrogen and oxygen species (such as H_2O_2, superoxide) [21]. Therefore, we further studied the inhibitory effect of LMWHA-MPB NPs on proliferation and migration of 4T1 cells *in vitro*.

First of all, the wound healing assay was constructed to study the inhibitory effect on cell motility. As illustrated in **Figure 4A** and **B**, after incubation for 18 h, the migration rates of 4T1 cells in

normal serum-free medium, M2 conditioned medium, MPB pre-treated M2 conditioned medium and LMWHA-MPB pre-treated M2 conditioned medium were 32.3 ± 3.54%, 53.9 ± 6.99%, 50.6 ± 4.71% and 13.1 ± 1.72%, respectively. This result indicated after reversing TAMs phenotype by LMWHA-MPB NPs, the migration behavior of highly metastatic 4T1 tumor cells can be effectively inhibited. Then, transwell assay was conducted to further study the effect of LMWHA-MPB on invasion and metastasis ability of 4T1 cells. The results were presented in **Figure 4C** and **D**. Cells incubating with normal medium, M2 conditioned medium and MPB pre-treated M2 conditioned medium passed through the upper compartment transwell and covered almost the entire lower surface of the membrane. The invasion rates in M2 conditioned medium and MPB pre-treated M2 conditioned medium groups were 1.81 ± 0.14 and 1.66 ± 0.16, indicating M2 macrophages could obviously promote the migratory and invasive ability of 4T1 cells. On the contrary, after co-culture with LMWHA-MPB pre-treated M2 conditioned medium, the invasion and metastasis ability of 4T1 cells sharply decreased from 1.81 ± 0.14 to 0.25 ± 0.03. Moreover, the main correlated cytokines had also been determined. As **Figure S9** shown, after incubation with LMWHA-MPB pre-treated M2 conditioned medium for 24 h, the expression of tumor metastasis-associated markers in 4T1 cells, such as MMP-9 and VEGF, were significantly reduced in comparison with the control and M2 groups. All above data suggested that LMWHA-MPB NPs treated M2 macrophages exhibited great potential in anti-metastatic effects on 4T1 cells.

Cytotoxicity study with LMWHA-MPB/HMME *in vitro*

In vitro cytotoxicity of LMWHA-MPB/HMME was determined using SRB method. **Figure 4E** demonstrated MPB NPs (50 μg/mL) had a little toxicity (~83% survival rate) on 4T1 cells, and ultrasound irradiation alone showed no obvious cytotoxicity (~94% survival rate). However, LMWHA-MPB pre-treated conditioned medium displayed obvious tumor killing effect with cell viability of 65.8 ± 2.1%. After HMME loading, the viability sharply reduced to 22.1 ± 2.8%. Then calcein AM/PI staining was conducted to visualize the sonodynamic cytotoxicity. As **Figure 4F** shown, compared with MPB NPs, the number of dead cells (red) in LMWHA-MPB group increased significantly. While in LMWHA-MPB/HMME group, almost all tumor cells were killed combining with ultrasound irradiation. These results were in agreement with cell viability assay as mentioned above. This indicated LMWHA-MPB with the ability of macrophage phenotypic transformation could significantly enhance the SDT effect of HMME.

NIR imaging to explore the targeting ability of LMWHA-MPB NPs

A sufficient distribution amount in targeted tumor is a prerequisite for LMWHA-MPB NPs to achieve its biological effects. The noninvasive NIR optical imaging technique was applied to estimate the biodistribution of LMWHA-MPB. IR783, a NIR dye, was encapsulated into LMWHA-MPB (LMWHA-MPB/IR783) for NPs tracking *in vivo*. The real-time images were recorded in **Figure 5A**. Free IR783 was lack of tumor targeting ability and mainly accumulated in liver. Furthermore, its fluorescence weakened gradually with time, suggesting free IR783 could be cleared easily *in vivo*. On the contrary, LMWHA-MPB/IR783 NPs accumulated rapidly in tumor region at 2 h post injection, and the fluorescence signal was still strong up to 24 h, indicating the notable tumor targeting and accumulation abilities of LMWHA-MPB. At 24 h, mice were sacrificed. The major organs and tumor tissues were harvested for ex vivo imaging. As **Figure 5B** and **5C** shown, LMWHA-MPB/IR783 demonstrated significantly enhanced fluorescence signals in tumor site and reticuloendothelial system (RES), such as liver, spleen and lung tissues. Moreover, there was also obvious fluorescence of IR783 in kidneys. This is because a part of IR783 that loaded into LMWHA-MPB will leak out as free dye molecules during *in vivo* circulation, and then they are cleared through kidneys. The notable tumor targeting ability could be elucidated by MPB-mediated EPR effect based on its nanoscale size as well as CD44 receptor-mediated active targeting endocytosis.

US imaging based on O_2 production

This study intended to explore the SDT enhancement effect of LMWHA-MPB through increasing tumor local O_2 level. As we known, solid tumor has a hypoxic microenvironment, which seriously affects SDT efficacy. Enhancing tumor oxygen partial pressure is a key method to improve SDT efficiency. As reported by many studies, cancer cells have been found to generate oxidative stress by producing an elevated level of H_2O_2 [23, 24]. Moreover, as presented in **Figure S10**, MPB NPs owned good catalase activity. LMWHA modification did not affect this characteristic. In order to visually monitor O_2 generation in tumor sites, the Vevo2100 small animal US imaging system was used to obtain US signal images *in vitro* and *in vivo*. **Figure 5D** proved O_2 production in the catalytic reaction of MPB

NPs and H_2O_2 could be clearly recorded using US images. **Figure 5E** showed at 2 h post injection, notable US signals appeared in MPB and LMWHA-MPB groups, suggesting there was plenty of O_2 in tumor tissues. Furthermore, it was noteworthy that the signal intensity in LMWHA-MPB treated tumor was much stronger than that of MPB treated tumor. This may be due to the macrophage phenotypic remodeling characteristics of LMWHA-MPB NPs. We had proved that LMWHA-MPB could remodel M2 to M1 phenotype. M1-like phenotype can secrete pro-inflammatory oxygen species, such as H_2O_2 [21], to ensure sufficient endogenous substrate (H_2O_2) supplement. To confirm this hypothesis, we further tested the concentration of H_2O_2 in three different macrophages. Results in **Figure S11** proved that after being induced by LMWHA-MPB NPs, the amount of H_2O_2 in M1-like phenotypes increased significantly. All these data suggested LMWHA-MPB NPs not only had excellent tumor targeting capability to deliver drug, but also owned O_2 self-provided characteristic at tumor sites.

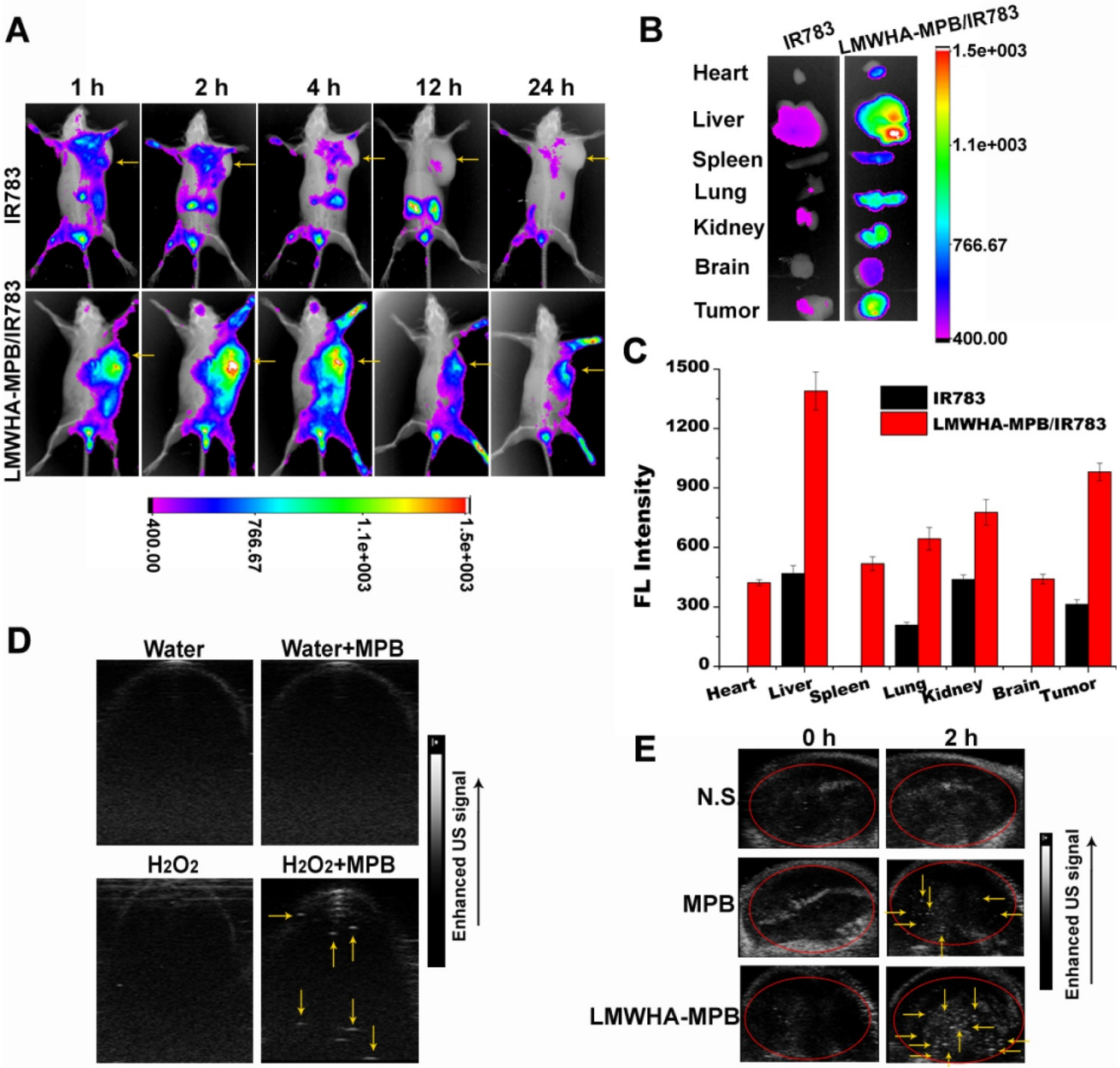

Figure 5. (**A**) *In vivo* NIR imaging of 4T1 tumor-bearing mice after the intravenous injection of free IR783 solution and IR783 labeled LMWHA-MPB NPs at 2, 12 and 24 h. Tumor tissues are indicated by yellow arrows. (**B**) Ex vivo NIR imaging of various major tissues in different groups at 24 h post injection. (**C**) Fluorescence intensity statistics of various tissues. (**D**) *In vitro* US imaging based on O_2 production during the reaction of MPB NPs (10 μg/mL) and H_2O_2 (2 mM). US signals are indicated by yellow arrows. (**E**) *In vivo* US imaging of tumors at different time points after intravenous injection of N.S., MPB and LMWHA-MPB NPs into 4T1 tumor-bearing mouse model. Tumor tissues are indicated by red circle and US signals are indicated by yellow arrows.

In vivo antitumor studies

The promising properties of tumor targeting and O_2 self-producing displayed by LMWHA-MPB NPs *in vivo* led us to explore the enhanced tumor SDT effect. HMME was chose as the model drug. During 10 days of treatment, changes of relative tumor volume (V/V_0) for each group were summarized in **Figure 6A**. The visual image of tumor tissues after the mice were sacrificed can be seen in **Figure S12**. LMWHA-MPB demonstrated a modesty tumor inhibition. This was mainly because LMWHA-MPB could remodel TAMs phenotypes (pro-tumor M2→ anti-tumor M1). M1 macrophages are conducive to inhibit tumor proliferation by secreting pro-inflammatory cytokines (such as TNF, IL-6, IL-12, and IL-23), reactive nitrogen and oxygen species (such as H_2O_2, superoxide) [21]. Free HMME and LMWHA-MPB groups showed similar tumor growth trends. Nevertheless, LMWHA-MPB/HMME displayed the best therapeutic efficacy with a reduced relative tumor volume of 0.31 ± 0.19 at day 11, which was much lower than free HMME or LMWHA-MPB group alone. ROS is the main active substance that achieves tumor SDT. Therefore, we measured in site ROS amount after administration. As shown in **Figure S13**, comparing with the extremely low ROS level in HMME group, LMWHA-MPB/HMME could significantly increase therapeutically active ROS amount in tumor site. This result suggested that LMWHA-MPB/HMME could achieve O_2 self-supplied SDT and enhanced anti-tumor effect of HMME significantly *in vivo*. What's more, mice treated with LMWHA-MPB/HMME exhibited no weight loss (**Figure 6B**). The histological changes of tumor tissues were tested by H&E staining **(Figure 6C**). It could be observed a compact cell arrangement in N.S. group, whereas cell shrinkage and expanding intercellular space emerged in HMME, LMWHA-MPB and MPB/HMME groups. Furthermore, LMWHA-MPB/HMME group displayed apparent cell lysis and necrosis as well as wide tumor cell disappearance areas, implying a remarkable antitumor activity.

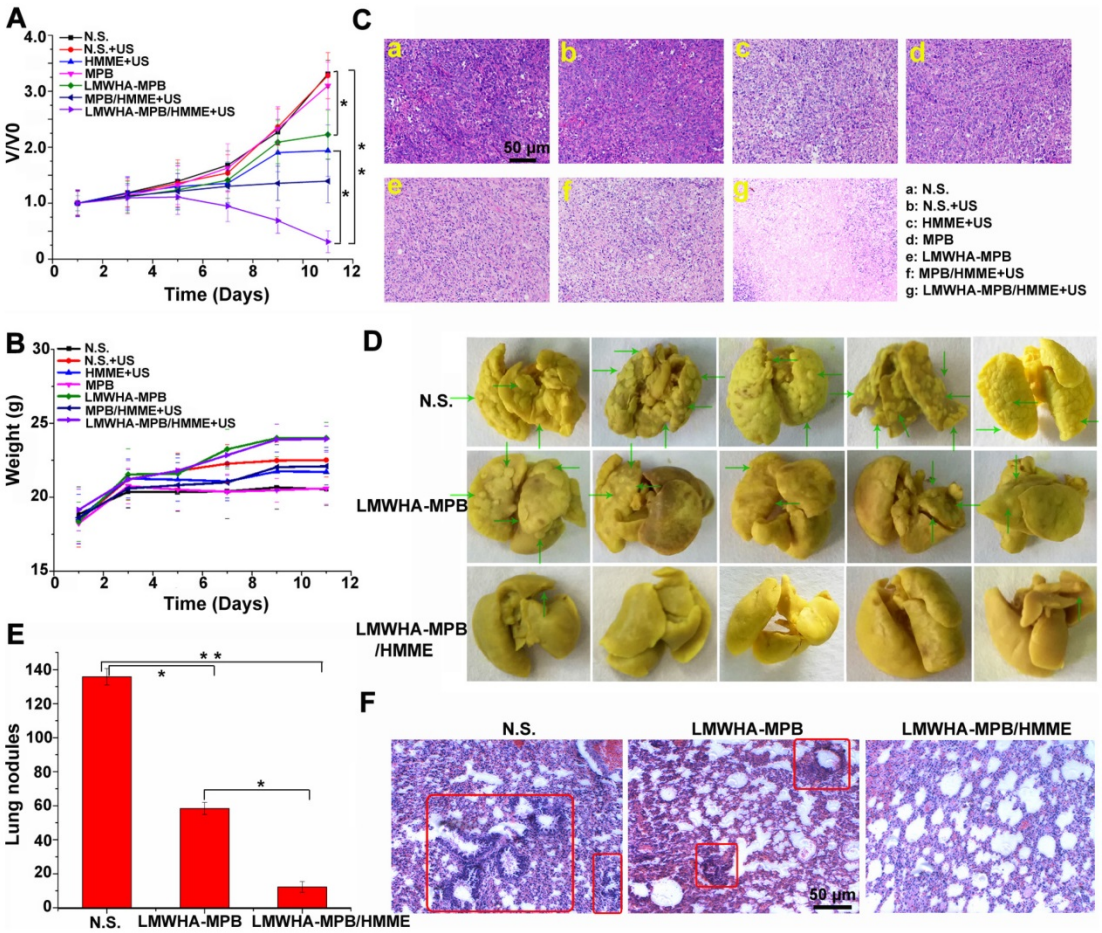

Figure 6. (**A**) The variation of relative tumor volume during treatment in different groups. (**B**) Changes of body weight measured during treatment in different groups. (**C**) H&E stained tumor tissues harvested from the mice with different treatments. (**D**) Photographs of the lungs in different groups. The nodules are indicated by green arrows. (**E**) The number of tumor nodules in the lungs. (**F**) H&E stained lung tissues harvested from the mice with different treatments. The metastasis of 4T1 tumors in lung are indicated by red box. (*P < 0.05 and **P < 0.01).

In vitro results demonstrated the remarkable anti-tumor migration and metastatic abilities of LMWHA-MPB NPs on 4T1 cells. So at the endpoint of pharmacodynamic experiment, the lung tissues in N.S, LMWHA-MPB and LMWHA-MPB/HMME+US groups were isolated to evaluate the pulmonary metastasis of 4T1 tumor. As shown in **Figure 6D** and **E**, the pulmonary nodules in LMWHA-MPB group (58.4 ± 3.6) were significantly less than those of N.S. group (135.8 ± 4.8). There were only 12.2 ± 2.4 pulmonary nodules in LMWHA-MPB/HMME group. Furthermore, H&E staining results of lung tissues were showed in **Figure 6F**. The metastasis of 4T1 tumors in lung were indicated by red box. In N.S. group, many tumor metastases were visible. Compared with normal lung tissue, metastatic tumor cells were closely arranged, with large and deep nuclear staining, as well as alveolar reduction. In LMWHA-MPB group, tumor metastases on the slice decreased significantly. In LMWHA-MPB/HMME group, there were almost no obvious metastases. All above results indicated that LMWHA-MPB/HMME could effectively inhibit the proliferation and metastasis of 4T1 tumor *in vivo*.

Furthermore, the polarization of TAMs, MMP-9, Ki67 and local hypoxia that associated with tumor proliferation and metastasis were evaluated by immunofluorescence staining. As shown in **Figure 7A** and **B**, in comparison with N.S. and N.S.+US groups, the percentages of M2 macrophages in LMWHA-MPB and LMWHA-MPB/HMME groups significantly decreased, while that of pro-inflammatory M1 macrophages increased. This trend was similar with *in vitro* results, implying that LMWHA-MPB NPs could successfully skew TAMs away from the M2 phenotype to the tumoricidal M1 phenotype. MMP-9 is a matrix metalloproteinase produced by macrophages, in response to stimulation by tumor derived factors. Studies have shown that tumor cells at primary sites induce the expression of MMP-9 and Ki67 in macrophages, which promote tumor cell establishment and proliferation in the metastatic cascade [30]. As **Figure 7A** and **C** shown, comparing with N.S. group, the expression of MMP-9 and Ki67 in LMWHA-MPB and LMWHA-MPB/HMME groups decreased, indicating the reduced metastasis ability of tumor. Moreover, angiogenesis is also closely related to tumor growth, invasion and metastasis. Shima et al. have proved that matrix metalloproteinase, such as MMP-9, is directly related to angiogenesis and metastasis [31]. So next, we studied the expression of CD31 (vascular endothelial cell marker) in tumor tissues. As **Figure S14** shown, the expression of CD31 in LMWHA-MPB group was down-regulated significantly, and among all groups, LMWHA-MPB/HMME+US group exhibited the lowest CD31 expression.

As we all know, hypoxia is a major feature of tumor microenvironment that limits SDT efficacy severely. In this study, we designed an O_2 self-supplied SDT system to alleviate tumor hypoxia and inhibit tumor progression. As shown in **Figure 7A** and **D**, after treated with LMWHA-MPB and LMWHA-MPB/HMME for 10 days, local tumor hypoxia situation had improved. This was because the remodeling effect of LMWHA-MPB on TAMs phenotypes (pro-tumor M2→anti-tumor M1) could produce high level of H_2O_2, which react with LMWHA-MPB to produce large amount of O_2, to efficiently manipulate the tumor microenvironment. After SDT, the degree of hypoxia in the tumor site was slightly elevated in LMWHA-MPB/HMME+US group. This is because consumption of O_2 during SDT can reduce the local O_2 partial pressure [32].

Finally, the potential toxicity of LMWHA-MPB *in vivo* was evaluated by the serum biochemistry assay and histological examination on health mice. As shown in **Figure S15** and **S16**, after administration at the therapy dose, all the parameters were normal, and no notable lesion or inflammation appeared in the major organs. Hence, LMWHA-MPB could be a kind of safe nanocarriers for cancer therapy or drug delivery.

Conclusion

In this study, LMWHA-MPB NPs were successfully synthesized as an in site macrophages converter and O_2 generator, to achieve the transformation of tumor microenvironment. *In vitro* and *in vivo* results demonstrated LMWHA-MPB NPs could remodel the polarization of M2 phenotype toward to M1 phenotype and improve O_2 level in tumor via catalytic decomposition of endogenous H_2O_2. Based on this characteristic, LMWHA-MPB NPs were explored as a kind of multifunctional biomaterials to realize O_2 self-supplied SDT of highly metastatic 4T1 tumors. *In vivo* anti-tumor results proved HMME loaded LMWHA-MPB drug delivery system (LMWHA-MPB/HMME) could effectively inhibit the proliferation and metastasis of 4T1 tumor by improving the tumor microenvironment.

Acknowledgements

This work was supported by grants from the National Natural Science Foundation of China (No. 81573364 and U1704172), and Key Program for Science and Technology Research in Henan Province (192102310153).

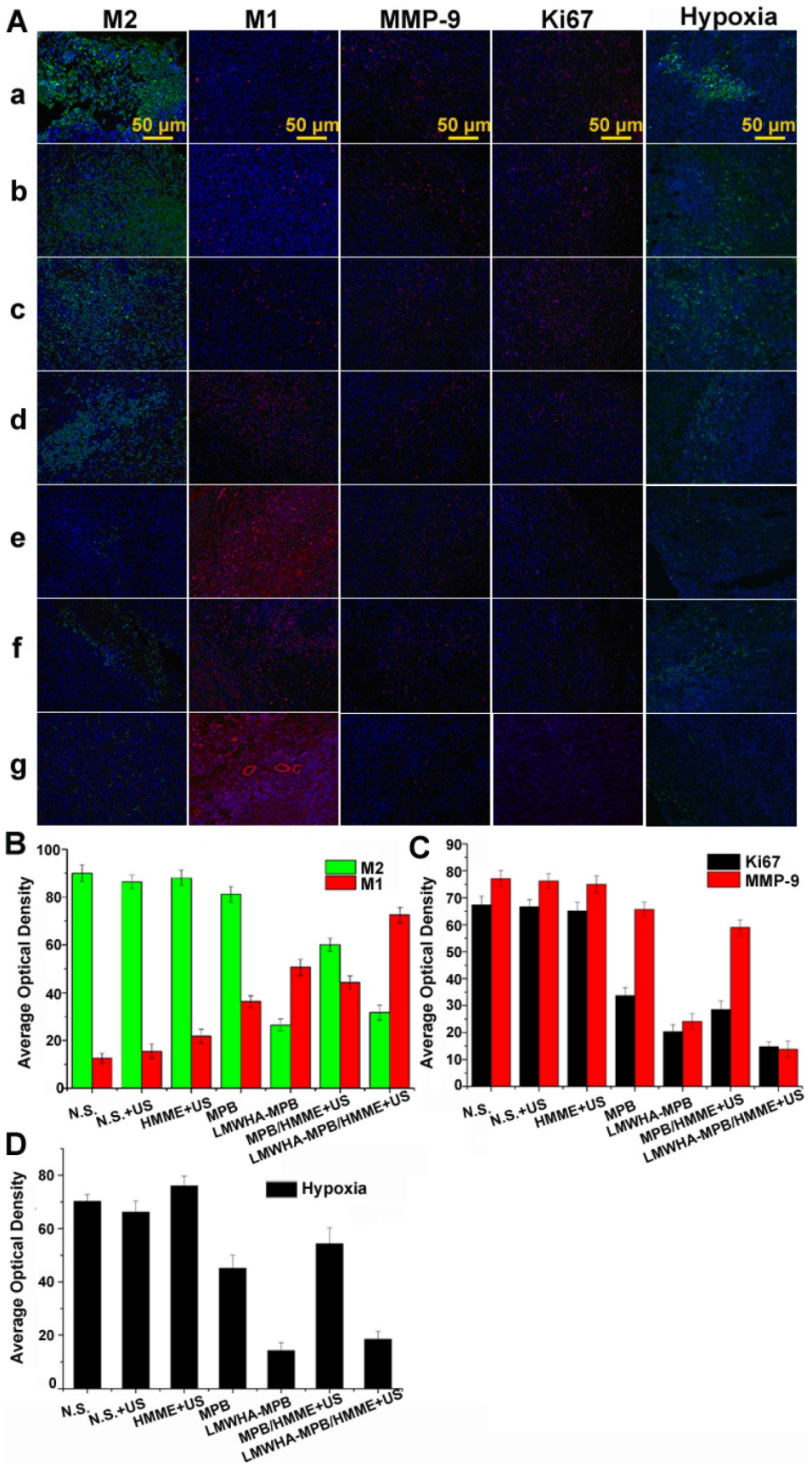

Figure 7. (**A**) Representative immunofluorescense images of tumor slices stained by CD206 (M2), CD86 (M1), MMP-9, Ki67 and Hypoxia maker, respectively. (a: N.S.; b: N.S.+US; c: HMME+US; d: MPB; e: LMWHA-MPB; f: MPB/HMME+US; g: LMWHA-MPB/HMME+US). (**B**) The quantitative AOD values of M1 and M2 in histogram. (**C**) The quantitative AOD values of Ki67 and MMP-9 in histogram. (**D**) The quantitative AOD values of hypoxia marker in histogram.

Supplementary Material

Supplementary figures and tables.
http://www.thno.org/v09p3580s1.pdf

Competing Interests

The authors have declared that no competing interest exists.

References

1. Jeong SK, Kim JS, Lee CG, Park YS, Kim SD, Yoon SO, et al. Tumor associated macrophages provide the survival resistance of tumor cells to hypoxic microenvironmental condition through IL-6 receptor-mediated signals. Immunobiology. 2017; 222: 55-65.
2. Silva VL, Al-Jamal WT. Exploiting the cancer niche: Tumor-associated macrophages and hypoxia as promising synergistic targets for nano-based therapy. J Control Release. 2017; 253: 82-96.
3. Tevis KM, Cecchi RJ, Colson YL, Grinstaff MW. Mimicking the tumor microenvironment to regulate macrophage phenotype and assessing chemotherapeutic efficacy in embedded cancer cell/macrophage spheroid models. Acta Biomater. 2017; 50: 271-9.
4. Zhou RY, Wang HM, Yang YF, Zhang CY, Dong XH, Du JF, et al. Tumor microenvironment-manipulated radiocatalytic sensitizer based on bismuth heteropolytungstate for radiotherapy enhancement. Biomaterials. 2019; 189: 11-22.
5. Patel A, Sant S. Hypoxic tumor microenvironment: Opportunities to develop targeted therapies. Biotechnol Adv. 2016; 34: 803-12.
6. Casey SC, Amedei A, Aquilano K, Azmi AS, Benencia F, Bhakta D, et al. Cancer prevention and therapy through the modulation of the tumor microenvironment. Semin Cancer Biol. 2015; 35: S199-S223.
7. Arroyo-Crespo JJ, Arminan A, Charbonnier D, Balzano-Nogueira L, Huertas-Lopez F, Marti C, er al. Tumor microenvironment-targeted poly-L-glutamic acid-based combination conjugate for enhanced triple negative breast cancer treatment. Biomaterials. 2018; 186: 8-21.
8. Semenza GL. Hypoxia-Inducible factors in physiology and medicine. Cell. 2012; 148: 399-408.
9. Chang Q, Jurisica I, Do T, Hedley DW. Hypoxia predicts aggressive growth and spontaneous metastasis formation from orthotopically grown primary xenografts of human pancreatic cancer. Cancer Res. 2011; 71: 3110-20.
10. Dewhirst MW, Cao Y, Moeller B. Cycling hypoxia and free radicals regulate angiogenesis and radiotherapy response. Nat Rev Cancer. 2008; 8: 425-37.
11. Yang J, Li W, Luo LH, Jiang MS, Zhu CQ, Qin B, et al. Hypoxic tumor therapy by hemoglobin-mediated drug delivery and reversal of hypoxia-induced chemoresistance. Biomaterials. 2018; 182: 145-56.
12. Wang HR, Chao Y, Liu JJ, Zhu WW, Wang GL, Xu LG, et al. Photosensitizer-crosslinked in-situ polymerization on catalase for tumor hypoxia modulation & enhanced photodynamic therapy. Biomaterials. 2018; 181: 310-7.
13. Zhang HJ, Chen JJ, Zhu X, Ren YP, Cao F, Zhu L, et al. Ultrasound induced phase-transition and invisible nanobomb for imaging-guided tumor sonodynamic therapy. J Mater Chem B. 2018; 6: 6108-21.
14. Song XJ, Feng LZ, Liang C, Yang K, Liu Z. Ultrasound triggered tumor oxygenation with oxygen-shuttle nanoperfluorocarbon to overcome hypoxia-associated resistance in cancer therapies. Nano Lett. 2016; 16: 6145-53.
15. Chen Q, Feng LZ, Liu JJ, Zhu WW, Dong ZL, Wu YF, et al. Intelligent albumin-MnO_2 nanoparticles as pH-/H_2O_2-responsive dissociable nanocarriers to modulate tumor hypoxia for effective combination therapy. Adv Mater. 2016; 28: 7129-36.
16. Liu CP, Wu TH, Liu CY, Chen KC, Chen YX, Chen GS, et al. Self-supplying O_2 through the catalase-like activity of gold nanoclusters for photodynamic therapy against hypoxic cancer cells. Small. 2017; 13: 1700278.
17. Song ML, Liu T, Shi CR, Zhang XZ, Chen XY. Bioconjugated manganese dioxide nanoparticles enhance chemotherapy response by priming tumor-associated macrophages toward M1-like phenotype and attenuating tumor hypoxia. Acs Nano. 2016; 10: 633-47.
18. Jordan BF, Sonveaux P. Targeting tumor perfusion and oxygenation to improve the outcome of anticancer therapy. Front Pharmacol. 2012; 3: 94.
19. Feng QH, Li YZ, Yang XM, Zhang WX, Hao YW, Zhang HL, et al. Hypoxia-specific therapeutic agents delivery nanotheranostics: A sequential strategy for ultrasound mediated on-demand tritherapies and imaging of cancer. J Control Release. 2018; 275: 192-200.
20. Yin W, Qiang M, Ke WD, Han Y, Mukerabigwi JF, Ge ZS. Hypoxia-responsive block copolymer radiosensitizers as anticancer drug nanocarriers for enhanced chemoradiotherapy of bulky solid tumors. Biomaterials. 2018; 181: 360-71.
21. Zhong XM, Chen B, Yang ZW. The Role of Tumor-associated macrophages in colorectal carcinoma progression. Cell Physiol Biochem. 2018; 45: 356-65.
22. Nath A, Pal R, Singh LM, Saikia H, Rahaman H, Ghosh SK, et al. Goldmanganese oxide nanocomposite suppresses hypoxia and augments pro-inflammatory cytokines in tumor associated macrophages. Int Immunopharmacol. 2018; 57: 157-64.
23. Szatrowski TP, Nathan CF. Production of large amounts of hydrogen peroxide by human tumor cells. Cancer Res. 1991; 51: 794-8.
24. Gao WW, Avila BEF, Zhang LF, Wang J. Targeting and isolation of cancer cells using micro/nanomotors. Adv Drug Deliv Rev. 2018; 125: 94-101.
25. Peng JR, Yang Q, Li WT, Tan LW, Xiao Y, Chen LJ, et al. Erythrocyte-membrane-coated prussian blue/manganese dioxide nanoparticles as H_2O_2-responsive oxygen generators to enhance cancer chemotherapy/photothermal therapy. ACS Appl Mater Inter. 2017; 9: 44410-22.
26. Toole BP. Hyaluronan: from extracellular glue to pericellular cue. Nat Rev Cancer. 2004; 4: 528-39.
27. Rayahin JE, Buhrman JS, Zhang Y, Koh TJ, Gemeinhart RA. High and low molecular weight hyaluronic acid differentially influence macrophage activation. ACS Biomater Sci Eng. 2015; 1: 481-93.
28. Hu M, Furukawa S, Ohtani R, Sukegawa H, Nemoto Y, Reboul J, et al. Synthesis of prussian blue nanoparticles with a hollow interior by controlled chemical etching. Angew Chem Int Edit. 2012; 51: 984-8.
29. Kamat M, El-Boubbou K, Zhu DC, Lansdell T, Lu XW, Li W, et al. Hyaluronic acid immobilized magnetic nanoparticles for active targeting and imaging of macrophages. Bioconjug Chem. 2010; 21: 2128-35.
30. Rogers TL, Holen I. Tumour macrophages as potential targets of bisphosphonates. J Transl Med. 2011; 9: 177.
31. Zeynali-Moghaddarn S, Mohammadian M, Kheradmand F, Fathi-Azarbayjani A, Rasmi Y, Esna-Ashari O, et al. A molecular basis for the synergy between 17-allylamino-17-demethoxy geldanamycin with capecitabine and irinotecan in human colorectal cancer cells through VEFG and MMP-9 gene expression. Gene. 2019; 684: 30-8.
32. Zhang HJ, Chen JJ, Zhu X, Ren YP, Cao F, Zhu L, et al. Ultrasound induced phase-transition and invisible nanobomb for imaging-guided tumor sonodynamic therapy. J Mater Chem B. 2018; 38: 6108-21.